Nonlinear viscoelastic analysis of a cylindrical balloon squeezed between two rigid moving plates

Andrea de Simone, Angelo Luongo

Nonlinear viscoelastic analysis of a cylindrical balloon squeezed between two rigid moving plates

Andrea De Simone, Angelo Luongo *

Università degli Studi dell'Aquila, Dipartimento di Ingegneria Civile, Edile-Architettura ed Ambientale, Via Giovanni Falcone 25, 67100 Coppito (AQ), Italy

A B S T R A C T

A nonlinear model of visco elastic balloon, interposed between a couple of moving rigid bodies, is formu lated. The pneumatic structure is modeled as a thin, infinitely long cylindrical membrane, pre stressed by an internal pressure. External pressure is assumed to be zero. The pushing bodies are modeled as a couple of frictionless rigid parallel plates, approaching each other normally, and causing squeezing of the pneu matic body. Motion is assumed to be slow, in such a way that any inertial effects are negligible. Both cases of long and short plates are considered, the latter entailing the possibility of puncture of the deformable body. A thermoplastic polyurethane material behavior is considered, and proper constitutive relation ships adopted. Several models are formulated, which differ for constitutive laws (inextensible, elastic, lin early or non linearly visco elastic) and/or for kinematic description (small strains and displacements or finite kinematics). The governing mixed differential algebraic equations are analytically or numerically integrated for several impressed motion time histories and the main features of the phenomenon are investigated.

1. Introduction

Pneumatic structures have many applications in different tech nical fields. Often, they consist in balloons interposed between bodies of higher stiffness, that cause their squeezing or puncture. Examples are fender devices, gaskets, balloons for bulkheads con trol, blood vessels, circulatory system and angioplasty balloons. Fender devices are used in nautical, such as peer fenders, ship fenders and rollers; pressurized gaskets are interposed between bodies in contact; balloons are used to lift up bulkheads, to create artificial rapids for rafting. Balloons are also extensively used for biomedical applications, e.g. to free narrowed arteries obstructed by cholesterol or fats in general, and in ocular biomechanics (Ross and Simmons, 2007). In marine engineering, and especially for high speed marine vehicles, the problem of mitigation of impact of the vessel over the water surface and the hydroelasticity of inflatable boats involves the contact of pressurized membrane with water and other elastic structures (e.g., Hirdaris and Temarel, 2009; Car caterra and Ciappi, 2004).

The squeezing and/or puncture of balloon involves a lot of phys ical phenomena, whose mathematical modeling is far from being accomplished, yet, although it has been developed in different con texts, as sketched below. (a) Usually one thinks to a balloon as a flexible membrane, whose narrow thickness remains constant in space and time. However, large strains could trigger local change in thickness, requiring a more refined model of 3D body, or a 2D model endowed with an interface, e.g. as done in Dell'Isola and Romano (1986) and Dell'Isola and Kosinski (1993). (b) Simi larly, the small bending stiffness could be important to describe wrinkles manifesting at, or close to, the contact regions, e.g. as studied in Yokota et al. (2001), with reference to membranes. (c) The repeated folding of the membrane, caused by contact with an obstacle, could damage the material, entailing changes in the mechanical characteristics. The relevant investigation calls for using methods of Continuum Damage Mechanics (Lemaitre and Chaboche, 1998), or for detection of solid solid phase transitions (e.g., Altenbach and Eremeyev, 2008a,b; Eremeyev and Pie traszkiewicz, 2009, 2011; Dell'Isola and Romano, 1986, 1987). In these cases, phenomena occurring at the nanoscale cannot be ig nored (see Altenbach et al. (2012) and Dell'Isola et al. (2012) for theoretical investigations, and Rinaldi et al., 2010a,b, for experi mental tests). (d) When a balloon is squeezed, the included gas mi grates outwards, depending on porosity of the material, thus possibly affecting the performance of the pneumatic structure. Mechanics of porous media should be invoked, along the lines of (Dell'Isola and Batra, 1997; Quiligotti et al., 2003; Coussy, 2004; Dell'Isola et al., 2003). (e) The mechanics of the contact necessarily involves dynamics effects, that should be thoroughly investigated, as e.g. done in Andreaus and Nisticò (1998), Andreaus and Casini (2001).

* Corresponding author. Tel.: +39 0862 434521.

E-mail addresses: andrea.desimone@univaq.it (A. De Simone), angelo.luongo@in-g.univaq.it (A. Luongo).

In spite of such a complicated problem, quite coarse models have been so far adopted. They mostly concern initially flat membranes in adhesive state with a solid, while few papers have been devoted to closed membranes impacting a solid. Here, a short overview of these latter is given. In Ligarò and Barsotti (2008), an effective method has been proposed for determining the equilibrium shapes of closed pressurized membranes under various inhomogeneous boundary conditions. By referring to new high performance textile materials, an idealized two state behavior is postulated, for which the membrane is inextensible when in traction and free to contract when in compression. Both the planar and the axisymmetric problems have been addressed. The axisymmetric contact problem of a pressurized spherical membrane interposed between two (large) rigid plates has been first studied in Feng and Yang (1973), where the material is assumed nonlinear elastic, obeying to the Mooney law, and the stability problem is addressed. Very recently, the problem has been reconsidered in Nadler (2010), where the contact problem has been formulated in regime of large deformations, by accounting for general elastic isotropic strain energy, and general enclosed fluid. In that paper, the wrinkling phenomenon, which possibly occurs on a part of the contact area, has also been investigated. Successively, the model has been generalized in Sohail and Nadler (2011), to study large deformations generated by a rigid frictionless conical indenter. There, fluid has been assumed incompressible. In all these works, numerical methods have been used to integrate the resulting set of nonlinear ordinary differential equations governing the problem.

In this paper the planar problem is addressed, with the following aims: (1) to formulate a simple model, able to give insights into the physics of the phenomenon, via analytical or semi analytical solutions; (2) to account for visco elastic properties of the material, to be described at different levels of refinement; (3) to account both for flattening and indentation of the balloon, as sequential stages. To this end, a long cylindrical balloon under internal pressure is considered, interposed between two rigid plates, slowly approaching each other normally. External pressure is assumed zero. By ignoring boundary effects, the problem is studied as planar, in the plane orthogonal to the cylinder axis. The contact is assumed to be frictionless. Due to the prescribed motion of the plates, quasi static variations of geometry, tension, and internal pressure occur. The configuration history is sketched in Fig. 1, for both cases of 'long' (Fig. 1a) and 'short' (Fig. 1b) plates. Contact initially occurs at one point on each plate (phase I in Fig. 1a and b), then it extends over a segment during the loading process (phases II in Fig. 1a and b), while the free part of the membrane keeps its circular shape, with modified unknown radius. Phases I, II are common to both kind of plates, and will be referred to as the *flattening* of the balloon. If plates are long, the process, in principle, ends with a complete adhesion of the membrane to the plates (phase III), in which the balloon degenerates in a segment. Since this occurrence is physically not realizable, a configuration close to (but not at) the complete adhesion has been represented in Fig. 1a. If, in contrast, plates are short, a transition configuration is observed (phases III in Fig. 1b), in which the adherent part of the membrane entirely cover the plates, while a part is free, but with the balloon still lying in the region delimited the two plates. Successively, a puncture of the deformable body occurs, in which a part of the balloon bulges behind the plates (phase IV in Fig. 1b), ending with a complete puncture (phase V in Fig. 1b). Phases IV and V will be referred to as indentation of the balloon.

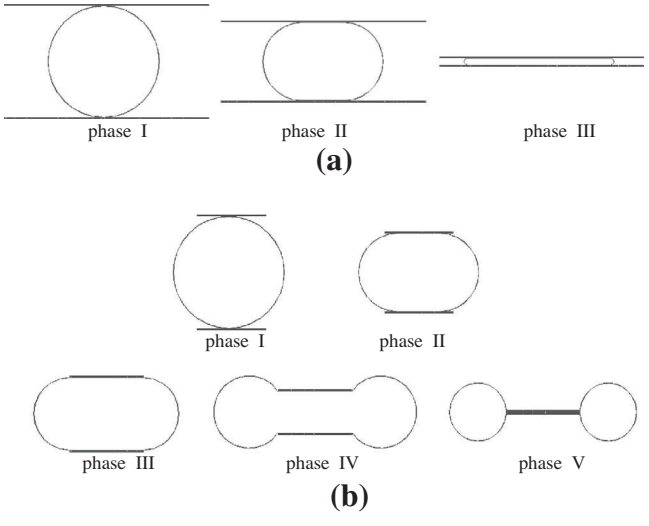

Fig. 1. Evolution of the membrane configuration: (a) long plates: (I) initial contact, (II) partial contact, (III) advanced configuration (close to total adhesion); (b) short plates: (I) initial contact, (II) partial contact, (III) transition configuration, (IV) punctured configuration, (V) final configuration (totally punctured).

The whole analysis is carried out in quasi static regime, by accounting for visco elastic behavior. The balloon is assumed to be made of polymeric material (e.g., Mc Crum et al., 1997), for which different enhanced visco elastic laws are considered, with large strains also accounted for (Qi and Boyce, 2005; Bergstrom and Boyce, 1998). The models were first implemented in De Simone (2010) and relevant preliminary results presented in De Simone and Luongo (2011); here, a refinement of the formulation and numerical simulations is accomplished.

The paper is organized as follows. In Section 2 the model is formulated for a generic constitutive law. In Section 3, this is specialized to (a) inextensible, (b) elastic, (c) linear visco elastic, (d) large strain visco elastic, (e) fully nonlinear visco elastic membranes. In Section 4 numerical results are illustrated and commented. In Section 5 some conclusions are drawn. In the appendix a pre contact evolution analysis is developed.

2. Planar model of cylindrical membrane

2.1. General equations

An infinitely long, homogeneous, cylindrical membrane of z axis is considered, whose thickness h is small with respect the length of the directrix (Fig. 2a). Boundary conditions and forces are assumed to be independent of z, so that the problem can be studied in the (x, y) plane. A direct, 2 D model of membrane is formulated, in which stress and strains along the normal to the middle surface are ignored, and thickness is included in the constitutive law.

An initial configuration $\mathcal{C}_I$, assumed known, is taken as reference configuration (Fig. 2b). In it, a material point P is identified by the (material) abscissa S, and its position by the vector $\mathbf{X}(S)$. In the current configuration $\mathcal{C}_t$ assumed by the membrane at time t, the point P occupies the new position $\mathbf{x} = \mathbf{x}(S, t)$ (time t understood ahead). The initial length of the segment dS: = $||d\mathbf{X}||$ changes into ds: = $||d\mathbf{x}||$ = $||\mathbf{x}'||dS$, where the dash denotes differentiation with respect to S (or s, if proper). The stretch λ : ds/dS, or, equivalently, the elongation ε : λ 1 (also said 'engineering strain'), is assumed as a strain measure:

$$\varepsilon \quad \|\mathbf{x}'(S)\| \quad 1 \tag{1}$$

By denoting by $\mathbf{a}_t$ $\mathbf{x}'(s) \equiv \mathbf{x}'(S)/\lambda(S)$ and $\mathbf{a}_n$ the unit vectors, respectively tangent and (outwards) normal to the curve $\mathcal{C}_t$ at P, the local *curvature*, in the spatial coordinate, reads $R^{-1}(s)$: $\|\mathbf{a}'(s)\|$ $\|\mathbf{x}''(s)\|$, or in material coordinate $R^{-1}(S)$ $\|\mathbf{x}'(S)\times$

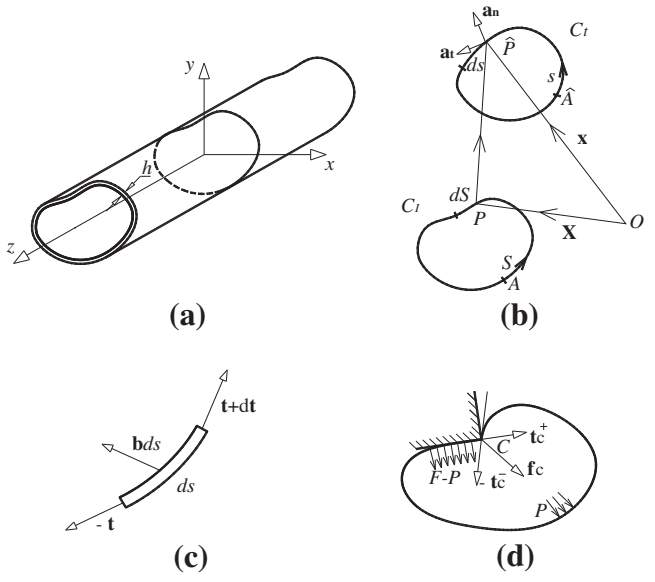

Fig. 2. Cylindrical membrane in planar state of stress: (a) 3D-view; (b) kinematics; (c) elemental equilibrium; (d) membrane pressed against a rigid obstacle.

$\mathbf{x}''(S)\|/\|\mathbf{x}'(S)\|^3$. The volume enclosed by the membrane per unit z length, having dimensions $[L^2]$ (and simply referred ahead *as the 'volume'*), in both forms, is:

$$V: \quad \frac{1}{2}\oint_{C_t}\mathbf{x}(s)\times\mathbf{x}'(s)\cdot\mathbf{a}_z ds \equiv \frac{1}{2}\oint_{C_I}\mathbf{x}(S)\times\mathbf{x}'(S)\cdot\mathbf{a}_z dS \tag{2}$$

where $\mathbf{a}_z$ is unit vector of the z axis.

The membrane is loaded by external body forces $\mathbf{b} = \mathbf{b}(\mathbf{x}; s, t)$, which depend on the unknown configuration, and have the dimensions of a force per unit of *current* area. Dependence on time is assumed slow, so that any dynamic effect can be neglected. Different contributions are distinguished, namely $\mathbf{b}: = P\mathbf{a}_n + \mathbf{b}_{out} + \mathbf{b}_r$, where: P is the (homogeneous) pressure exerted by an inflated gas normally to the walls of the membrane; $\mathbf{b}_{out}$ are outside active forces, for example due to an external fluid in which the membrane is immersed; and $\mathbf{b}_r$ are contact reactive forces exerted by an obstacle on a part of the membrane. The internal force $\mathbf{t}: = T\mathbf{a}_t$, having the dimension of a force per unit length, is taken as a measure of the stress of the membrane; its modulus T will be refereed as the 'tension' of the membrane. Equilibrium in the current configuration requires that $d\mathbf{t} + \mathbf{b}ds = \mathbf{0}$ (Fig. 2c), or, in material coordinate:

$$\mathbf{t}' + \lambda\mathbf{b} \quad 0 \tag{3}$$

where $\lambda\mathbf{b}$ is the body force referred to the unstretched area. Equilibrium, moreover, must be enforced at corners C at which the slope $\mathbf{x}'$ is discontinuous (see Fig. 2d), by requiring $\mathbf{t}_C^+ \quad \mathbf{t}_C + \mathbf{f}_C \quad 0$, where $\mathbf{f}_C$ is a reactive force.

To complete the problem, constitutive laws must be given. Concerning the material behavior, the law relates tension and strain, and, possibly, their time derivatives, namely:

$$f(T, \dot{T}, \varepsilon, \dot{\varepsilon}; T_I) \quad 0 \tag{4}$$

in which the pre tension T_I acts as a parameter. Eq. (4) must be sided by the initial conditions $T(S,0) \quad T_I(S),\ \varepsilon(S,0) \quad \varepsilon_I(S)$, where the index I denotes evaluation at $\mathcal{C}_I$. Gas is assumed to behave as a perfect gas under isothermal transformations, for which the Boyle law holds:

$$PV \quad P_I V_I \tag{5}$$

About reactive forces, it is assumed that the obstacle is friction less, for which the reaction $\mathbf{b}_r = F\mathbf{a}_n$ is purely normal. Consistently, reactions at the corners are assumed to act along the bisector of the angle formed by the two tangents, this entailing $\|\mathbf{t}_C^+\| \quad \|\mathbf{t}_C\|$, i.e. the tension keeps its modulus T constant trough the corner. Finally, $\mathbf{b}_{out}$ are data of the problem.

Eqs. (1) (5) constitute a partial differential system in the unknowns $\mathbf{x}(S,t)$, $P(t)$, $V(t)$, $T(S,t)$, $\varepsilon(S,t)$; boundary conditions require continuity of the position vector $\mathbf{x}$ and equilibrium at corners. The problem formally coincides with that which governs planar cables (see, e.g. Luongo et al., 1984).

A special, but important case occurs when no outside forces are applied to the membrane, i.e. $\mathbf{b}_{out} = \mathbf{0}$. Then, since $d\mathbf{a}_t/dS \quad \lambda R\ ^1\mathbf{a}_n$, the equilibrium Eq. (3) reads:

$$T'\mathbf{a}_t + \lambda\left(P + F \quad \frac{T}{R}\right)\mathbf{a}_n \quad 0 \tag{6}$$

The tangential equilibrium entails T = const on the free and on the in contact parts of the membrane; however, due to the equilibrium at the corners, T is constant throughout the membrane. The normal equilibrium condition, when written on the free surface (on which $F = 0$), reads $T = PR$. Since P and T are constant, it follows, that the radius R is also constant, i.e. the free surface has circular directrix. When the normal equilibrium is enforced on the contact surface, R is assigned, and the reaction is evaluated as $F = \quad P + T/R$; if the obstacle is flat, i.e. $R = \infty$, then $F = \quad P$, i.e. the pressure is entirely balanced by the reaction.

Concerning kinematics, due to the fact that tension is constant, even the strain ε is constant in the domain. Moreover, since the free part of the membrane is circular, the global quantity R and another geometrical parameter can be used to describe geometry, instead of the vector $\mathbf{x}(S)$. However, one of them must be taken as control parameter for the loading process, so that just one geometrical variable is unknown, conveniently taken as the radius R of the circular part.

In conclusion, when no outside forces act on the membrane, the original infinite dimensional problem can be formulated as a much simpler finite dimensional problem, in terms of the unknowns $\mathbf{q}(t): = (R(t), P(t), V(t), T(t), \varepsilon(t))$. If the material is visco elastic, the problem is mixed algebraic differential in time; if it is elastic, it further degenerates into algebraic.

2.2. Membrane compressed between two parallel plates

The problem described in the Introduction is now addressed. It consists of a long cylindrical membrane, inflated by gas, interposed between two planar rigid plates approaching each other along the normal direction.

The state of first contact between membrane and plates (phase I in Fig. 1) is taken as reference configuration. Here $\mathbf{q}_I: = (R_I, P_I, V_I, T_I, \varepsilon_I)$ are assumed to be known quantities. Their evaluation, of course, calls for solving a pre contact evolution problem, in which the cylindrical membrane freely evolves, after it has been insufflated (see the Appendix). This transformation leads the body from its natural state to the initial state, as a consequence of its own visco elastic properties.

By accounting for the double symmetry of the system, only a quarter of the membrane is considered, as shown in Fig. 3, for the two cases of long plates (Fig. 3a and b) and short plates (Fig. 3c ans d). In the initial configuration (Fig. 3a) the membrane is circular, of center O, and delimited by the (material) contact point A and the symmetry point C; the volume (per membrane unit length) subtended by this arc is $V_I \quad \pi R_I^2/4$. In the current configuration $\mathcal{C}_t$ (Fig. 3b and c), a third point B is of interest, which separates the in contact portion of the membrane (AB segment) from the circular part (BC arc). The projection of B on the horizontal symmetry axis is the new center O' of the arc. The current configuration is determined once the radius R and the angle $\theta \quad A\hat{O}B$ are

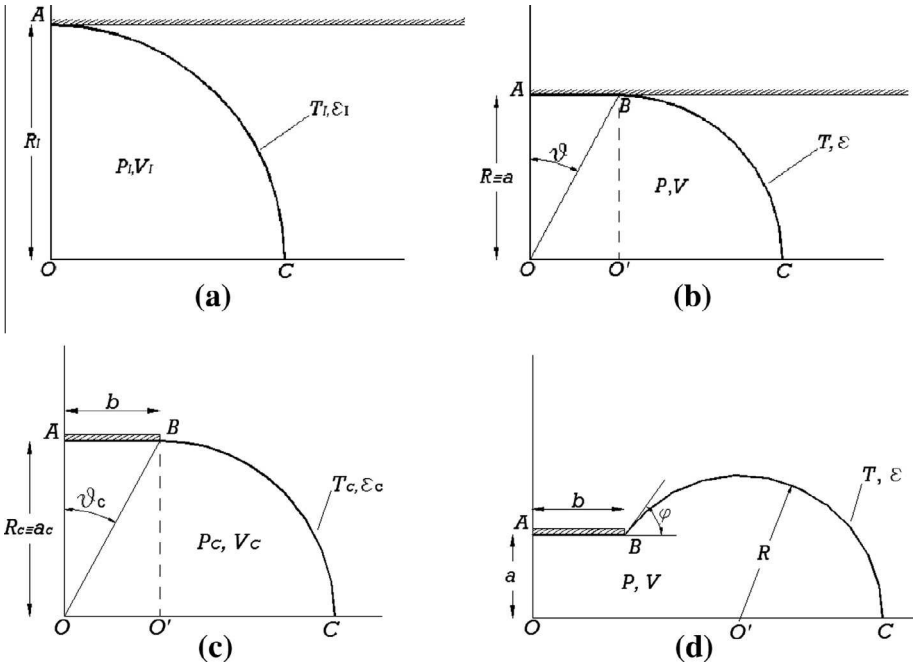

Fig. 3. Configurations and state variables for long (a and b) and short (c and d) plates: (a) initial state; (b) actual state; (c) transition state; (d) indentation configuration; θ, φ are control parameters.

known. Although R coincides with the (assigned) semi distance a between the two plates, it appears computationally more conve nient to take the angle θ, instead of R, as control parameter for the loading process, by leaving to R the meaning of configuration variable. This state, that also occurs for short plates, will be re ferred to as *flattening*.

If the plates are short, the system experiences a *transition* state $\mathcal{C}_C$ (here the index C remembers the incipient appearance of a corner) in which the contact point B coincides with an end of the plate (Fig. 3c); in this configuration the quantities previously introduced assume the values $\mathbf{q}_C$: = (R_C, P_C, V_C, T_C, ε_C). A further approach between the plates causes the new geometrical structure of Fig. 3d (indented con figuration). In order to describe how the phenomenon evolves, the new control parameter φ is chosen, which is the angle that the tan gent at the circular arc at point B forms with the horizontal axis. The center of the arc, O', is no more the projection of B, and therefore a and R are no more coincident, but $a = R\cos\varphi$. In this phase, the state variables will be still denoted by $\boldsymbol{q}$: = (R, P, V, T, ε), but the state will be referred to as indentation. The history of these quantities, as well as the instant at which the system reaches the transition config uration, now depends on the plate semi length b.

The problem described above is governed by the following set of equations:

$$
\begin{aligned}
&T \quad PR\\
&PV \quad P_IV_I\\
&f(T,\dot{T},\varepsilon,\dot{\varepsilon}) \quad 0\\
&V \quad \begin{cases} R^2(\tan\theta+\frac{\pi}{4}) & \text{in flattening}\\ \frac{R^2}{4}(\sin 2\varphi+\pi+2\varphi)+bR\cos\varphi & \text{in indentation}\end{cases}\\
&\varepsilon \quad \begin{cases} \frac{R}{R_I}(1+\frac{2}{\pi}\tan\theta) \quad 1 & \text{in flattening}\\ \frac{R}{R_I}(1+\frac{2}{\pi}\varphi)+\frac{2b}{\pi R_I} \quad 1 & \text{in indentation}\end{cases}
\end{aligned}
\tag{7}
$$

Here, Eqs. (7a,b,c) have already been introduced, expressing normal equilibrium, gas and membrane constitutive laws, respec tively; moreover, Eqs. (7d,e) are *volumetric* and *extensional* compat ibility equations, respectively. They are obtained by elementary calculations relevant to the shape assumed by the membrane in Fig. 3b and d. The indentation state, of course, only exists if the plates are short. In the transition state, $\tan\theta \quad b/R$, $\varphi \quad 0$, so that both the alternative expressions in Eqs. (7d) and (7e) furnish $V_C = bR + \pi R^2/4$ and $\varepsilon_C = R/R_I + (2b)/(\pi R_I)$, thus assuring continuity.

3. Specialized constitutive models and solutions

The governing Eq. (7) are specialized ahead to different consti tutive models of membrane, and solutions reported, when avail able in closed form. Non dimensional quantities are used, according to the following definitions:

$$
p: \quad P/P_I, \quad \tau \quad T/T_I, \quad v: \quad V/V_I, \quad r: \quad R/R_I \quad \alpha \quad a/R_I, \quad \beta \quad b/R_I \tag{8}
$$

in which $T_I = P_IR_I$ holds, since $\mathcal{C}_I$ is equilibrated.

3.1. Inextensible membrane

The simplest model of material behavior is the inextensible model. In this case, $\varepsilon \equiv 0$ and T assumes a reactive character (i.e. it would be a Lagrangian parameter in a variational formulation, in which $T\varepsilon = 0$ is enforced). Therefore, the relevant mechanical problem is governed by four equations in four unknowns. By using non dimensional quantities, they read:

$$
\begin{aligned}
&\tau \quad pr, \quad pv \quad 1,\\
&v \quad \begin{cases} r^2(1+\frac{4}{\pi}\tan\theta) \\ r^2(1+\frac{2}{\pi}\varphi+\frac{1}{\pi}\sin 2\varphi)+\frac{4}{\pi}\beta r\cos\varphi \end{cases}, \quad \begin{cases} r(1+\frac{2}{\pi}\tan\theta) \quad 1\\ r(1+\frac{2}{\pi}\varphi)+\frac{2}{\pi}\beta \quad 1\end{cases}
\end{aligned}
\tag{9}
$$

in the flattening and indentation states, respectively.

Eq. (9) admit a unique closed form solution. In the flattening state, it reads:

$$
r \quad \frac{\pi}{\pi+2\tan\theta}, \quad v \quad \frac{\pi(4\tan\theta+\pi)}{(2\tan\theta+\pi)^2},
$$
$$
p \quad \frac{(2\tan\theta+\pi)^2}{\pi(4\tan\theta+\pi)}, \quad \tau \quad 1 \quad \frac{2}{4+\pi\cot\theta} \tag{10}
$$

and in the indentation state:

$$
\begin{aligned}
r &\quad \frac{\pi \quad 2\beta}{\pi+2\varphi},\\
v &\quad \frac{(\pi \quad 2\beta)(4\beta(\pi+2\varphi)\cos\varphi+(\pi \quad 2\beta)(\pi+2\varphi+\sin 2\varphi))}{\pi(\pi+2\varphi)^2},\\
p &\quad \frac{\pi(\pi+2\varphi)^2}{(\pi \quad 2\beta)(4\beta(\pi+2\varphi)\cos\varphi+(\pi \quad 2\beta)(\pi+2\varphi+\sin 2\varphi))},\\
\tau &\quad \frac{\pi(\pi+2\varphi)}{4\beta(\pi+2\varphi)\cos\varphi+(\pi \quad 2\beta)(\pi+2\varphi+\sin 2\varphi)}
\end{aligned}
\tag{11}
$$

3.2. Elastic membrane

An improved model accounts for elasticity of the membrane. By assuming that the body obeys to the Hooke law, by using the engi neering strain ε, and accounting for the initial tension, the consti tutive relationship reads:

$$T \quad T_I + Eh_I\varepsilon \tag{12}$$

where E is the Young modulus and hIthe thickness, evaluated at C_I. In non dimensional form, the elastic problem (7) reads:

$$
\begin{aligned}
&\tau \quad pr, \quad p\nu \quad 1, \quad \tau \quad 1+k\varepsilon,\\
&\nu \quad \begin{cases} r^2\left(1+\frac{4}{\pi}\tan\theta\right)\\ r^2\left(1+\frac{2}{\pi}\varphi+\frac{1}{\pi}\sin 2\varphi\right)+\frac{4}{\pi}\beta r\cos\varphi \end{cases},\\
&\varepsilon \quad \begin{cases} r\left(1+\frac{2}{\pi}\tan\theta\right) \quad 1\\ (r+2\beta)\left(1+\frac{2}{\pi}\varphi\right) \quad 1 \end{cases}
\end{aligned}
\tag{13}
$$

in the two states, respectively. In Eq. (13) the following non dimen sional elastic stiffness has been introduced:

$$k: \quad Eh_I/T_I \tag{14}$$

Eq. (13) can still be solved analytically. They admit two distinct solutions; one of them, however, has to be disregarded, since phys ically not admissible, being $\tau < 0$ (see De Simone (2010) and De Si mone and Luongo (2011)). The admissible solution, instead, reads as follows: (a) in the flattening state:

$$
\begin{aligned}
&\tau \quad \frac{1}{2}\left(1 \quad k+\frac{\cos\theta A(\theta)B(\theta)}{\pi\cos\theta+4\sin\theta}\right),\\
&p \quad \frac{(1+k^2)\pi+4(1+(k \quad 1)k)\tan\theta \quad (k \quad 1)A(\theta)B(\theta)}{2\pi},\\
&\varepsilon \quad \frac{1}{2k}\left(\frac{B(\theta)}{A(\theta)} \quad 1 \quad k\right),\\
&\nu \quad \frac{\pi((1+k^2)\pi+4(1+(k \quad 1)k)\tan\theta+(k \quad 1)A(\theta)B(\theta))}{2k^2(\pi+2\tan\theta)^2},\\
&r \quad \frac{\pi\left(\quad 1+k+\frac{B(\theta)}{A(\theta)}\right)}{2k(\pi+2\tan\theta)}
\end{aligned}
\tag{15}
$$

and, (b) in the indentation state:

$$
\begin{aligned}
&\tau = \frac{\beta(\pi+2\varphi) \quad 2\beta(\pi+2\varphi)\cos\varphi+\beta\sin 2\varphi+\frac{1}{2}C(\varphi)}{\pi(\pi+2\varphi+\sin 2\varphi)},\\
&p = \frac{1}{\pi^3 \quad 8\pi\beta^2\cos\varphi}(\pi^3+2\pi^2\varphi+2\beta^2\pi(1 \quad 2\cos\varphi)\\
&+2\beta^2(2\varphi \quad 4\varphi\cos\varphi+\sin 2\varphi)+\beta C(\varphi)),\\
&\varepsilon = \frac{(\beta \quad \pi)(\pi+2\varphi) \quad 2\beta(\pi+2\varphi)\cos\varphi+(\beta \quad \pi)\sin 2\varphi+\frac{1}{2}C(\varphi)}{\pi(\pi+2\varphi+\sin 2\varphi)},\\
&\nu = \frac{1}{\pi(\pi+2\varphi)^2}(\pi^3+2\pi^2\varphi+2\beta^2\pi(1 \quad 2\cos\varphi)\\
&+2\beta^2(2\varphi \quad 4\varphi\cos\varphi+\sin 2\varphi) \quad \beta C(\varphi)),\\
&r = \frac{1}{(\pi+2\varphi)(\pi+2\varphi+\sin 2\varphi)}(\quad \beta\pi(1+2\cos\varphi)\\
&\quad 2\beta(\varphi+\cos\varphi(2\varphi+\sin\varphi))+\frac{1}{2}C(\varphi)\Big),
\end{aligned}
\tag{16}
$$

where the following functions of the control parameters have been defined:

$$
\begin{aligned}
&A(\theta): \quad \sqrt{\pi+4\tan\theta}, \quad B(\theta): \quad \sqrt{(1+k)^2\pi+4(1+k^2)\tan\theta}\\
&C(\varphi): \quad \sqrt{4(\pi+2\varphi)(\pi^2-8\beta^2\cos\varphi)(\pi+2\varphi+\sin 2\varphi)+4\beta^2((\pi+2\varphi)(1+2\cos\varphi)+\sin 2\varphi)^2}.
\end{aligned}
\tag{17}
$$

3.3. Linear visco elastic membrane

To account for slow time effects and for internal energy dissipa tion of the membrane, a visco elastic constitutive model must be used. As a first, simplest approach to the problem, the well known *linear* standard model (also called 'three parameter model', Fig. 4) is adopted.

By using the engineering strain ε, the relevant constitutive rela tionship is:

$$\begin{cases} \dot{T}+\frac{K_2}{\eta}T \quad (K_1+K_2)\dot{\varepsilon}+\frac{K_1K_2}{\eta}\varepsilon\\ T(0) \quad T_I, \quad \varepsilon(0) \quad \varepsilon_I \end{cases}, \tag{18}$$

where K_1, K_2, are elastic moduli (having dimensions of N/mm), and η a viscosity coefficient (having dimensions of N/mm/s). In non dimensional form, it reads:

$$\begin{cases} \dot{\tau}+\tau \quad (k_1+k_2)\dot{\varepsilon}+k_1\varepsilon\\ \tau(0) \quad 1, \quad \varepsilon(0) \quad \varepsilon_I \end{cases}, \tag{19}$$

where:

$$\tilde{t}: \quad (K_2/\eta)t, \quad k_1: \quad K_1/T_I, \quad k_2: \quad K_2/T_I \tag{20}$$

have been introduced, and where the dot now denotes differentia tion with respect the non dimensional time t (tilde dropped ahead). The visco elastic problem for the system is therefore governed by:

$$
\begin{aligned}
&\tau \quad pr, \quad p\nu \quad 1,\\
&\nu \quad \begin{cases} r^2\left(1+\frac{4}{\pi}\tan\theta\right)\\ r^2\left(1+\frac{2}{\pi}\varphi+\frac{1}{\pi}\sin 2\varphi\right)+\frac{4}{\pi}\beta r\cos\varphi \end{cases},\\
&\varepsilon \quad \begin{cases} r\left(1+\frac{2}{\pi}\tan\theta\right) \quad 1\\ (r+2\beta)\left(1+\frac{2}{\pi}\varphi\right) \quad 1 \end{cases},\\
&\dot{\tau}+\tau \quad (k_1+k_2)\dot{\varepsilon}+k_1\varepsilon,\\
&\tau(0) \quad 1, \quad \varepsilon(0) \quad \varepsilon_I.
\end{aligned}
\tag{21}
$$

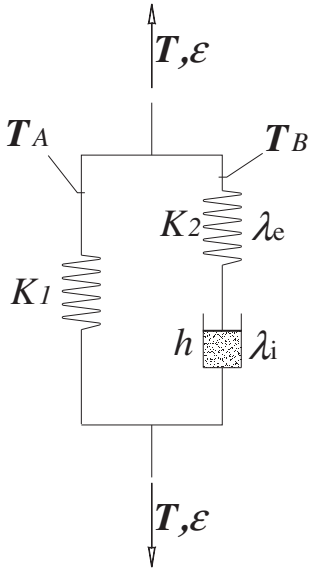

Fig. 4. Standard visco-elastic model.

It is a mixed differential algebraic problem, whose solution calls for a numeric integration. It can be recast in the matrix form:

$$\begin{cases} \mathbf{A}(\mathbf{y}(t))\dot{\mathbf{y}}(t) + \mathbf{B}(\mathbf{y}(t))\mathbf{y}(t) & \mathbf{f}(t) \\ \mathbf{y}(0) & \mathbf{y}_0 \end{cases} \tag{22}$$

where $\mathbf{A}$ and $\mathbf{B}$ are 6×6 matrices, $\mathbf{y} = (\mathbf{q};\ \theta)$or $\mathbf{y} = (\mathbf{q};\ \varphi)$is an extended 6 vector of state variables, including the control parameter, and $\mathbf{f}(t) = (1, 1, 0, \quad 1, 0; f(t))$ is a 6 vector of known terms, in which $f(t)$ denotes the impressed time history for $\theta(t)$ or $\varphi(t)$. Moreover $\mathbf{y}_0 = (r_I, p_I, v_I, \tau_I, \varepsilon_I; f(0))$. Eq. (22) have been integrated by using a solver for singular and sparse matrices.

3.4. Large strain visco elastic membrane

An enhanced visco elastic model is introduced, in which large strains are accounted for. The stretch $\lambda : \quad 1 + \varepsilon$ (whose logarithm is known as the 'true strain') instead of the elongation ε, is used as the strain measure, since this latter is not additive in finite kinematics.[1] Reference is made again to the three parameter model of Fig. 4, in which A is the elastic part and B the visco elastic part. Compatibility for the two parts requires $\lambda_A \quad \lambda_B \quad : \lambda$, while compatibility for part B calls for $\lambda \quad \lambda_i\lambda_e$, where $\lambda_{i,e}$ are the stretches of the in series inelastic and elastic devices, respectively. Equilibrium requires that $T = T_A + T_B$ and $T_i = T_e = :T_B$. By still assuming linear constitutive laws for the single devices, namely:

$$T_A \quad K_1(\lambda \quad 1), \quad T_B \quad K_2(\lambda_e \quad 1), \quad T_B \quad \eta\dot{\lambda}_i \tag{23}$$

the following nonlinear tension strain law is finally derived, with relevant initial conditions:

$$\begin{cases} \lambda\dot{T} \quad (K_1 + K_2 + T)\dot{\lambda} + \frac{K_2}{\eta}[T \quad K_1(\lambda \quad 1)]\left[1 \quad \frac{K_1}{K_2}(\lambda \quad 1) + \frac{T}{K_2}\right]^2 & 0 \\ T(0) \quad T_I, \quad \lambda(0) \quad \lambda_I \end{cases} \tag{24}$$

It should be noted that, for small strain and $T << K_2$, the squared bracket in Eq. (24) tends to 1, so that Eq. (18) is recovered. In non dimensional variables, Eq. (24) reads:

$$\begin{cases} \lambda\dot{\tau} \quad (k_1 + k_2 + \tau)\dot{\lambda} + [\tau \quad k_1(\lambda \quad 1)]\left[1 \quad \frac{k_1}{k_2}(\lambda \quad 1) + \frac{\tau}{k_2}\right]^2 & 0 \\ \tau(0) \quad \tau_I, \quad \lambda(0) \quad \lambda_I \end{cases} \tag{25}$$

The visco elastic problem for the large strain membrane model is therefore governed by the following set of equations:

$$\begin{aligned} &\tau \quad pr, \quad p\nu \quad 1, \\ &\nu \quad \begin{cases} r^2\left(1 + \frac{4}{\pi}\tan\theta\right) \\ r^2\left(1 + \frac{2}{\pi}\varphi + \frac{1}{\pi}\sin 2\varphi\right) + \frac{4}{\pi}\beta r\cos\varphi \end{cases}, \\ &\varepsilon \quad \begin{cases} r\left(1 + \frac{2}{\pi}\tan\theta\right) \quad 1 \\ (r + 2\beta)\left(1 + \frac{2}{\pi}\varphi\right) \quad 1 \end{cases}, \\ &\lambda\dot{\tau} \quad (k_1 + k_2 + \tau)\dot{\lambda} + [\tau \quad k_1(\lambda \quad 1)]\left[1 \quad \frac{k_1}{k_2}(\lambda \quad 1) + \frac{\tau}{k_2}\right]^2 \quad 0, \\ &\tau(0) \quad \tau_I, \quad \lambda(0) \quad \lambda_I. \end{aligned} \tag{26}$$

The whole system is then rearranged as in Eq. (22), to be numerically integrated.

[1] Indeed, if $\Delta l_1, \Delta l_2$ are two successive deformations of a segment of initial length l, then the final strain $\frac{\Delta l_1 + \Delta l_2}{l}$ differs from the sum of the two strains: $\varepsilon_1 \quad \frac{\Delta l_1}{l}$, $\varepsilon_2 \quad \frac{\Delta l_2}{l + \Delta l_1}$. In contrast, since $\lambda \quad \frac{l + \Delta l_1 + \Delta l_2}{l}$, $\lambda_1 \quad \frac{l + \Delta l_1}{l}$, $\lambda_2 \quad \frac{l + \Delta l_1 + \Delta l_2}{l + \Delta l_1}$, then $\lambda \quad \lambda_1\lambda_2$.

3.5. Fully nonlinear visco elastic membrane

Although the previous model accounts for large strains, the constitutive laws (23) of the single components are still linear. To formulate a fully nonlinear visco elastic model (i.e. large strain and mechanically nonlinear), it needs to describe more accurately the tension strain rate law. Here, reference is made to a thermoplastic polyurethane material, for which a proper 3D constitutive law, still based on the model of Fig. 4, has been proposed in Qi and Boyce (2005) and then reduced to a 1D law in De Simone (2010). It involves all the eigenvalues $\lambda_1, \lambda_2, \lambda_3$ of the deformation gradient $\mathbf{F}$. To reduce the model to 1D, two hypotheses are introduced: (a) *each* parts A and B are incompressible, and (b) the material is transversally isotropic, these entailing $\lambda_2 \quad \lambda_3 \quad \pm 1/\sqrt{\lambda}$, with $\lambda : \quad \lambda_1$ the longitudinal stretch. Although hypothesis (a) is quite strong (since isochoricity is more likely to hold on the two parts as a whole, rather than separately), it should be meant as a purely mathematical hypothesis, introduced here to keep the model the simplest possible. Based on these approximations, the following four parameter visco elastic 1D model were obtained in De Simone (2010) (quite involved details are omitted here):

$$T_A \quad c_1\left(\lambda^2 \quad \frac{1}{\lambda}\right), \quad T_B \quad c_2\frac{\ln\lambda_e}{\lambda_e}, \quad \frac{\dot{\lambda}_i}{\lambda_i} \quad c_3\left(\lambda_e\sqrt{1 + \frac{2}{\lambda_e^3}} \quad 1\right)^{c_4}\ln\lambda_e \tag{27}$$

in which c_i are constants depending on material. By using compatibility and equilibrium as in the previous model, the final constitutive equation was derived. Together with Eq. (26a d), they govern the fully nonlinear visco elastic problem for the membrane.

4. Numerical results

4.1. Parameter identification and material response

A preliminary identification of the constants has been carried out, by exploiting the results of experimental stretch tests performed by the first author on polyurethane samples at the Engineering Science Dept Laboratory of Oxford, UK (De Simone, 2010). Results of a strain controlled cycle test, conducted up to 300% maximum strain, at 0.03 s ^{1} strain rate, have been reported (by thin lines) in Fig. 5a and b. Additional experimental tests were also performed at strain rates ranging between 0.01 and 0.05 s ^{1}, whose results differed not more than 10 15%; therefore, reference was made to the average rate. The response consists of an almost linear elastic behavior, followed by an almost linear visco elastic phase, and a number of several hysteretic loops. Referring to the standard visco elastic model of Fig. 4, the three non dimensional parameters were identified as follows: (a) a secant elastic slope, able to capture the experimental stress corresponding to $\varepsilon = 0.25$ was attributed to the two in parallel springs as $K_1 + K_2$ (where $K_i : \quad K_i/h_I$, having the dimensions of a force per unit of area, refers to the material response, i.e. to the nominal stress $\sigma = T/h_I$ expressed as a function of the nominal strain ε); (b) the visco elastic slope was attributed to the stiffness K_1 of the A part (as a matter of fact, when $\dot{\varepsilon} \quad$ const and time is large, Eq. (18a) furnishes $\sigma \quad K_1\varepsilon + \text{const}$); (c) the viscosity parameter η was computed in order to fit, to the best extent, either (c_1) the area of the first loop (energy criterion), or (c_2) the maximum stress experienced. The results of the two identifications are displayed (by thick lines) in Fig. 5a and b, respectively. Identification based on the criterion of the maximum tension appears better than the one based on the energy criterion, and therefore has been adopted. The following numerical values for the material parameters were identified: $K_1 : \quad 1.8\ \text{N/mm}^2, K_2 : \quad 27\ \text{N/mm}^2, \eta \quad 160\ \text{N/mm}^2/\text{s},$ corre

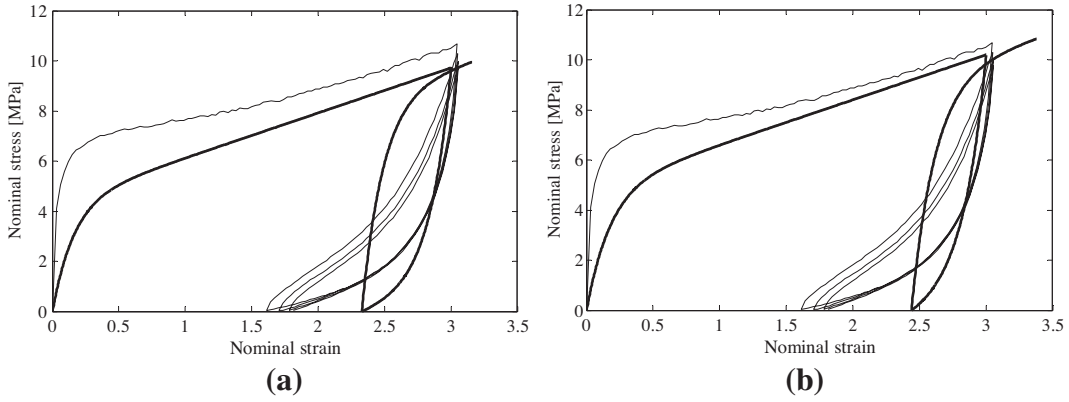

Fig. 5. Experimental stress–strain curve (thin lines) and Standard Model approximation (thick lines), according to the (a) equal area of loop criterion, (b) equal maximum tension criterion.

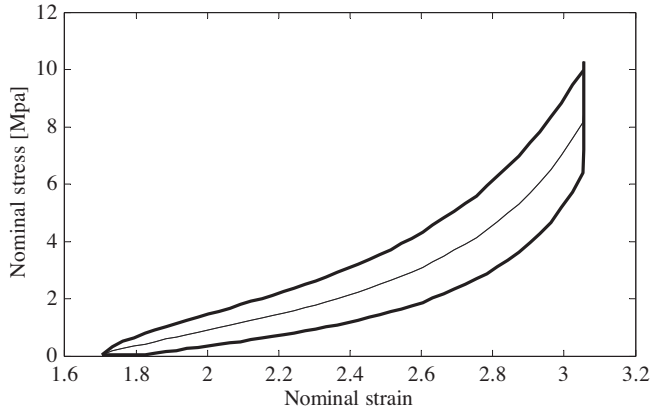

Fig. 6. Experimental first loop of hysteresis (thick lines) extracted by the plots of Fig. 4; the medium path (thin line) represents the hyperelastic experimental path while the upper path-medium path difference represents the effect of the viscosity.

sponding to the structural parameters K_1: = 1.8 N/mm, K_2: = 27 N/mm, η = 160 N/mm/s. They were used also for the large strain visco elastic model.

Concerning the fully nonlinear model, four constants have to be identified. To this end, a different method was used. Preliminary, the first loop of hysteresis was extracted by the plots of Fig. 5, and reported in Fig. 6 (thick lines). In it, the medium path (thin line), equidistant from the lower and upper branches, represents the hyperelastic experimental stress, while the difference between the upper and the medium paths represents the viscous stress contribution. In the theoretical model adopted, it can be shown that two out of four constants account for the hyperelastic behavior, while the remaining two for viscosity. Therefore, the following strategy was followed: the middle and the maximum values of the hyperelastic stress were measured, and two constants were chosen to reproduce them; moreover, the lower slope and the maximum value of the viscous stress were measured, and two constant used to reproduce them. As a result of the whole identification process, the following numerical values of parameters appearing in Eq. (27) were obtained: c_1 0.3 N/mm,c_2 50 N/mm,c_3 1 s^{-1},c_4 0.3.

In order to compare the responses of the three visco elastic constitutive laws formulated and identified above, the stress response to the same strain history was determined by numerically integrating the relevant constitutive laws (Fig. 7). Three models were considered, namely: the Linear Visco Elastic material (LVE, Eq. (19)), the Large Strain Visco Elastic material (LSVE, Eq. (25)) and the fully NonLinear Visco Elastic material (NLVE, Eq. (27)). The strain history (Fig. 7a) consists of a linear phase, followed by a quite long constant phase and finally a small amplitude harmonic phase. This example is meant to simulate a specific technical application, namely a fender ship which is insufflated, remains at the rest for a while, and then it is solicited with a harmonic law, due to a (idealized) boat rolling.

Fig. 7b shows the viscoelastic responses. When they are compared with the purely elastic behavior (not shown), a strong decay of the stress is noticed, due to the relaxation phenomenon occurring in the constant strain phase. The three models, however, give qualitatively similar results, although appreciable local differences exist. This entail that both geometrical (large strain) nonlinearities and constitutive nonlinearities slightly affect the material behavior. In particular, the LVE overestimate the peak reached at the end of ramp loading. However, at the end of the waiting phase, all models give the same response. During the successive harmonic loading, models give responses of the same period, but slightly different in amplitude and phase.

4.2. Structural response

The structural response of the balloon is now addressed (see Fig. 8). When $t < 0$, the balloon is at rest in its natural (unstressed, unstrained) configuration. At $t = 0$ an internal pressure P_0 is instantaneously applied by insufflating gas, so that the membrane undergoes the strain ε_0 and the tension T_0. With the gas flow stopped, a time interval is waited, in which, (a) if the membrane is elastic, tension and strain remain constant; (b) if the membrane is viscoelastic, the strain increases and the tension decreases (see the Appendix for pre contact analysis). At $t = t_I$ the balloon is in its initial state $\mathbf{q}_I = (r_I, p_I, v_I, \tau_I, \varepsilon_I)$, when it is put in one point contact with two parallel rigid plates. Then, the distance between the plates is reduced at a constant strain rate, and the response $\mathbf{q} = (r, p, v, \tau, \varepsilon)$ evaluated as a function of time. By bearing in mind a balloon for medical application, the following numerical values are assumed: semi width of the plate b = 30 mm, natural radius of the balloon R_N = 30 mm, thickness h = 1 mm, elastic modulus E = 28.8 MPa, inflating pressure (see the Appendix) P_0 = 0.10 MPa, initial (nondimensional) time t_I = 16.7; the aspect ratio (at the initial state) is found to be $\beta = b/R_I$ = 0, 54 for the LVE model and 0.90 for the E one. Relevant results are plotted in Fig. 8, for the Inextensible (I) and Elastic (E) models, for which closed form solution exists (Eqs. (10), (11), (15), and (16) respectively), and for the Linear Visco Elastic model, which follows numerical integration of Eq. (22). The flattening state is common to the two plates; at point C, however, the behavior differs, being still of flattening type for long

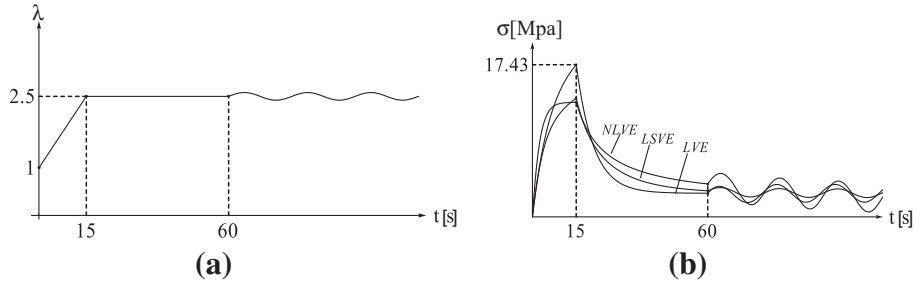

Fig. 7. Comparison between LVE, LSVE and NLVE constitutive laws: (a) strain-history, (b) stress-response.

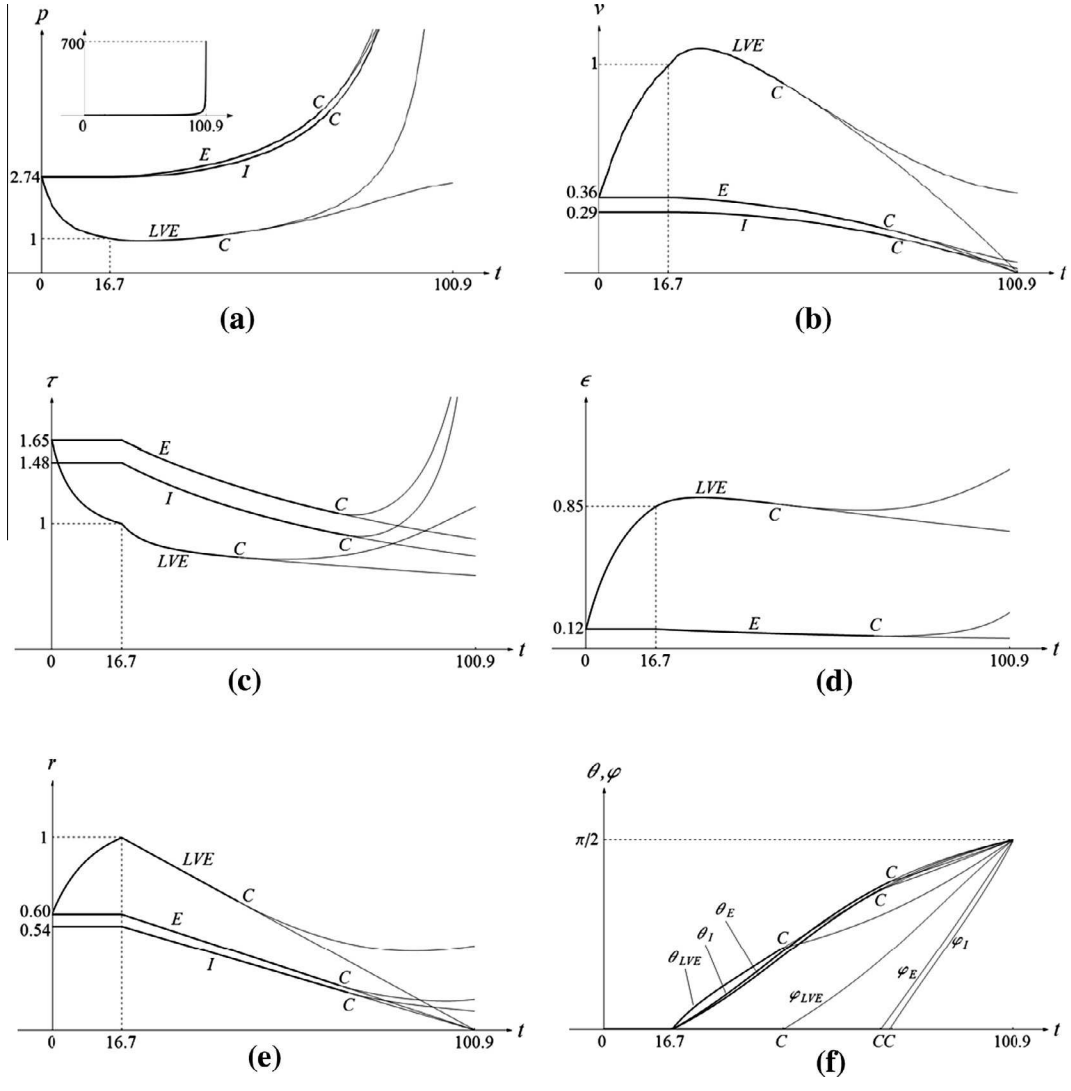

Fig. 8. Structural response of a balloon squeezed between long (thick lines) or short (thin lines) plates, moving with constant rate; C transition point; I inextensible, E elastic, LVE Linear Visco-elastic models); (a) pressure; (b) volume; (c) tension; (d) strain; (e) radius; (f) control parameters.

plates, and of indentation type for short plates. As a general com ment, the visco elastic response strongly differs from the elastic and inextensible ones, thus highlighting the importance to prop erly take into account the viscous component of the material. Spe cifically, during flattening, it is observed that radius and tension decrease, while volume, pressure and strain have not monotonic behavior, this being dependent on the material viscosity vs. load ing rate relationship. If the material viscosity has a prevalent ef fect, the volume and the strain increase and the pressure decreases (see Fig. 8b, in which the volume actually increases just after flattening phase start). On the other hand, if the loading ef fects prevail, the volume decrease and the pressure increases (see the elastic response in Fig. 8b, in which the viscous effects are absent and the volume, consequently, decreases). The growth of pressure, related to the decrease of volume, is statically balanced by the increase of curvature of the circular part of the balloon, although the tension decreases. The more the squeezing proceeds, the more the tension relaxes. This apparent relaxation, however, is

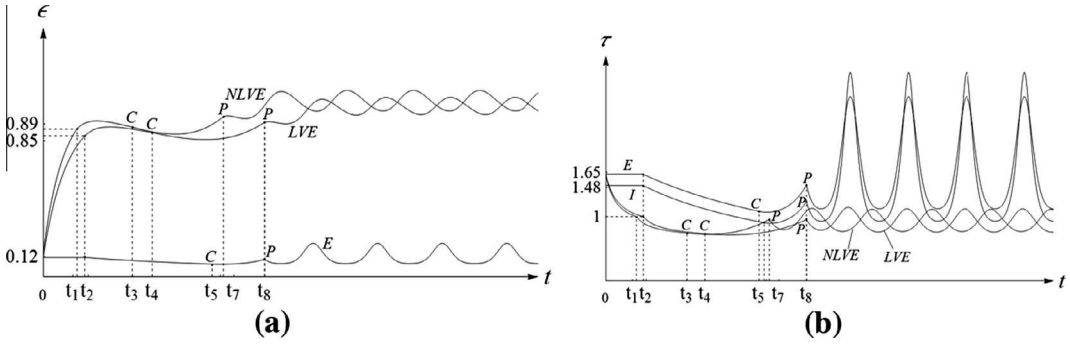

Fig. 9. Time-histories of (a) strain and (b) tension for resting/constant-rate/harmonic motion of the plates; *I*: inxstensible, *E*: elastic, *LVE*: linear visco-elastic, *NLVE*: linear visco-elastic; *I*, *P* constant-rate and harmonic motion starts, *C* transition point; $t_1 = 13.6$, $t_2 = 16.7$, $t_3 = 36.2$, $t_4 = 44.2$, $t_5 = 68.3$, $t_6 = 70.8$, $t_7 = 72.9$ and $t_8 = 89.4$.

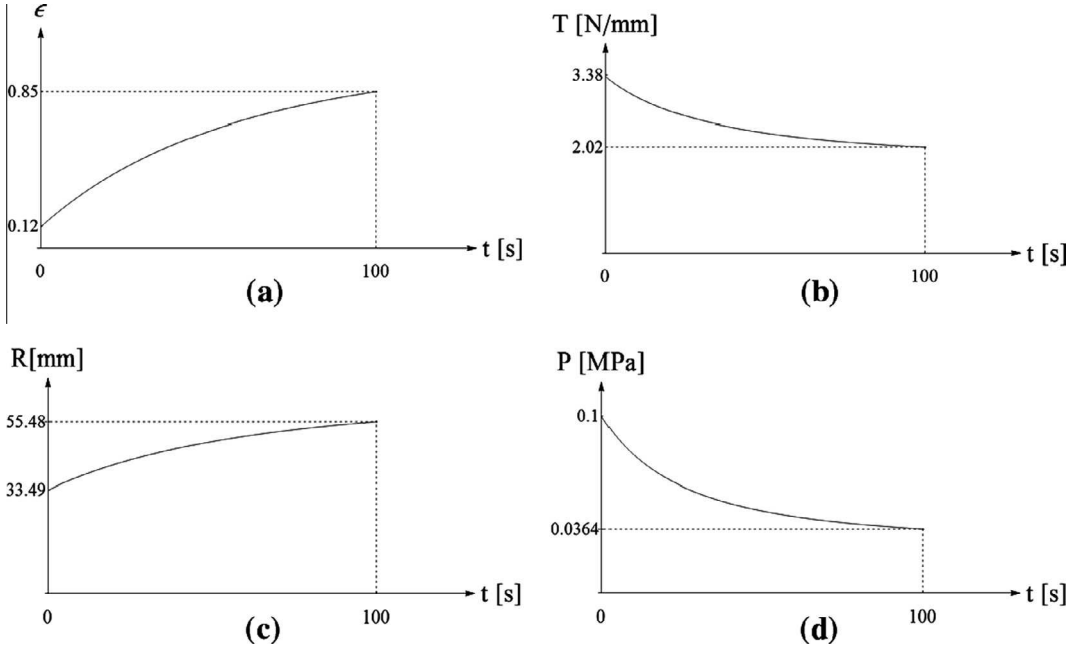

Fig. 10. State evolution in pre-contact phase for the LVE model; (a) strain; (b) tension; (c) radius; (d) pressure.

due to geometrical aspects of the structural problem, and not to the material behavior. During indentation, the previous trend is confirmed only during a very short initial stage, since strain and tension, successively, rise up. At the non dimensional time 100.9, the non dimensional pressure is very large (see the insert in Fig. 8a), while the volume is very small.

As a last simulation, a more complex displacement history has been imposed for the same balloon, and the results obtained for four models have been compared, namely: inextensible (I), elastic (E), linear visco elastic (LVE) and fully nonlinear viscoelastic (NLVE). Fig. 9 shows, for the four models, the strain (Fig. 9a) and the tension (Fig. 9b) time histories, including the pre contact phase. At the instant t_I, two short plates are juxtaposed to the bal loon, touching it each in a single point, and a constant rate mutual approach is imposed to them. Transition configuration is reached at an instant t_C which is different for each model. After that, the constant rate motion is continued for an additional time interval, sufficient to move the system far from the transition condition. Successively, at time t_P, a harmonic plate movement is started, of amplitude such that the balloon remains in the indentation state. As already observed, the elastic and inextensible responses strongly differ from the viscoelastic ones, giving much higher re sponses. In contrast, the linear and nonlinear viscoelastic models have quite similar behaviors. During the initial phases, it is seen that, while the tension decreases, the strain firstly decreases, but then it raises, as an effect of the viscoelasticity.

5. Conclusions

A nonlinear planar model of visco elastic cylindrical balloon, interposed between two approaching rigid plates, has been formu lated. The problem has been found to be governed by five alge braic ode equations in five state variables (radius, strain, volume, tension, internal pressure), expressing equilibrium, compatibility and tension strain rate relationships. The distance between the plates (or an equivalent geometrical magnitude) has been taken as loading parameter, and an arbitrarily selected time history, as signed. According to the ratio between the radius of the balloon and the length of the plates, a one phase evolution problem (only squeezing, for long plates) or a two phases evolution problem (first squeezing, then indentation, for short plates), occur. Five specific models have been derived, of increasing complexity: inextensible, linearly elastic, linear visco elastic, large strain visco elastic, fully nonlinear visco elastic. In the second and third model, the

elongation was taken as a measure of the strain, while in the fourth and fifth model the stretch was used.

By exploiting results of an experimental test, carried out on a polyurethane material, the parameters have been identified, and the responses of different constitutive models compared. It has been found that viscosity strongly affects the response, since the material is extremely sensible to the relaxation phenomenon. However, moderate differences were notice about the three vis co elastic models, to within enforced elongations of 150%, although local differences were appreciable.

The structural response has been evaluated for two different squeezing processes of the balloon. Again, the elastic and inexten sible responses predict tensions which are much higher than the viscoelastic ones, these latter being closer among them.

As a final remark, complex nonlinear constitutive laws have been found unnecessary in the technical applications investigated here (i.e. the fender ship and the angioplasty balloon), since the strain is not too high. On the other hand, it is believed that the non linear model could be useful in other applications, where larger strains are involved, still to be investigated.

Acknowledgements

This work was granted by the Italian Ministry of University and Research (MIUR), under the PRIN10 11 program, project N. 2010MBJK5B.

Appendix A. Pre-contact evolution analysis

It has been assumed, so far, that the initial state $\mathbf{q}_I := (R_I, P_I, V_I, T_I, \varepsilon_I)$, at which the plates are in a one point contact with the balloon, is known. Indeed, a specific pre contact analysis must be performed, to study the evolution of the balloon from its tension free natural state to the stressed initial state. Two phases are distinguished in such a process, namely: (a) the inflating phase, and (b) the evolution phase. At the first stage, the balloon is open and inflated by gas, up when a pre fixed internal pressure P_0 (measured by a manometer) is reached, and the balloon is closed. This phase is short, if compared with the whole evolution time interval, so that it can be considered as instantaneous, occurring at $t = 0$. The successive stage, instead, develops in a finite time interval $(0, t_I)$, which precedes the squeezing phase. During this interval, the state of the balloon freely evolves, ruled by the visco elastic properties of the mate rial. Pre contact analysis, therefore, is aimed to evaluate the inflating state, $\mathbf{q}_0 := \mathbf{q}(0)$, and the evolving state, $\mathbf{q}(t)$, $0 \leqslant t \leqslant t_I$, up to the initial state $\mathbf{q}_I := \mathbf{q}(t_I)$.

When the internal pressure is zero, the balloon assumes an arbi trary configuration described by a closed curve of given length l_N; among the infinite ones, we choose the circumference of radius $R_N := l_N/(2\pi)$. Since tension and strain also vanish in the natural state, it is $\mathbf{q}_N := (R_N, 0, V_N, 0, 0)$, with $V_N \quad \pi R_N^2$.

(a) Inflating state. When the pressure P_0 is instantaneously ap plied, it needs to distinguish inextensible and elastic (or visco elas tic) models. In the inextensible case, the equilibrium Eq. (1) is sufficient to determine the tension:

$$T_0 \quad P_0 R_N \tag{A.1}$$

so that $\mathbf{q}_0 := (R_N, P_0, V_N, T_0, 0)$. If, however, the balloon is elastic, the inflating state obeys to the following equations:

$$T_0 \quad P_0 R_0, \quad T_0 \quad E h_N \varepsilon_0, \quad \varepsilon_0 \quad R_0/R_N \quad 1 \tag{A.2}$$

which describe equilibrium, constitutive law (with Eh_N the stiffness in the natural state) and kinematics, respectively. Eq. (A.2) admit the solution:

$$T_0 \quad \frac{P_0 R_N}{1 \quad \frac{P_0 R_N}{E h_N}}, \quad \varepsilon_0 \quad \frac{P_0 R_N}{E h_N} \frac{1}{1 \quad \frac{P_0 R_N}{E h_N}}, \quad R_0 \quad \frac{R_N}{1 \quad \frac{P_0 R_N}{E h_N}}, \tag{A.3}$$

and therefore $\mathbf{q}_0 : \quad (R_0, P_0, V_0, T_0, \varepsilon_0)$, with $V_0 \quad \pi R_0^2$.

(b) *Evolving state*. With the balloon closed, and no external forces applied, its shape remains circular. Moreover, the state $\mathbf{q}_0$ does not evolve, if the model is inextensible or elastic, but changes in time if it is visco elastic. In this latter case, the equations govern ing the evolutions are:

$$T \quad PR, \quad PV \quad P_0 V_0, \quad f(T, \dot{T}, \varepsilon, \dot{\varepsilon}) \quad 0, \quad \varepsilon \quad R/R_N \quad 1, \quad V \quad \pi R^2 \tag{A.4}$$

expressing equilibrium, constitutive laws and kinematics, respec tively. By integrating Eq. (A.4) with the initial conditions $\mathbf{q}(0) = \mathbf{q}_0$, the state $\mathbf{q}(t) := (R(t), P(t), V(t), T(t), \varepsilon(t))$ at the instant t is evaluated, up to the time t_I. Fig. 10 shows the evolution for the LVE model, when the sample system of Section 4.2 is considered.

References

Altenbach, H., Eremeyev, V.A., 2008a. A. Analysis of the viscoelastic behavior of plates made of functionally graded materials. Math. Mech. 88, 332–341.

Altenbach, H., Eremeyev, V.A., 2008b. On the bending of viscoelastic plates made of polymer foams. Acta Mech. 204, 137–154.

Altenbach, H., Eremeyev, V.A., Morozov, N.F., 2012. Surface viscoelasticity and effective properties of thinwalled structures at the nanoscale. Int. J. Eng. Sci. 59, 83–89.

Andreaus, U., Casini, P., 2001. Forced motion of friction oscillators limited by a rigid or deformable obstacle. Mech. Struct. Mach. 29 (2), 177–198.

Andreaus, U., Nisticò, N., 1998. An analytical-numerical model for contact-impact problems: theory and implementation in a two-dimensional distinct element algorithm. Comput. Model. Simul. Eng. 3 (2), 98–110.

Bergstrom, J.S., Boyce, M.C., 1998. Constitutive modeling of the large strain time dependent behavior of elastomers. J. Mech. Phys. Solids 46, 931–954.

Carcaterra, A., Ciappi, E., 2004. Hydrodynamic shock of elastic structures impacting on the water: theory and experiments. J. Sound Vib. 271, 411–439.

Coussy, O., 2004. Poromechanics. John Wiley and Sons, Chichester.

De Simone, A., 2010. A non linear viscoelastic pneumatic 2D structure interposed between a couple of rigid moving surfaces, Ph.D. Thesis, University of L"Aquila.

De Simone, A., Luongo A., 2011. Nonlinear Viscoelastic Analysis of a pneumatic 2D structure interposed between a couple of rigid moving planes. Compdyn 2011, III Eccomas, Corfu, Greece.

Dell'Isola, F., Batra, R., 1997. Saint-Venant″s problem for porous linear elastic materials. J. Elast. 47, 73–81.

Dell'Isola, F., Kosinski, W., 1993. Deduction of thermodynamic balance laws for bidimensional nonmaterial directed continua modelling interphase layers. Arch. Mech. 45, 333–359.

Dell'Isola, F., Romano, A., 1986. On a general balance law for continua with an interface. Ricerche Mat. 35, 325–337.

Dell'Isola, F., Romano, A., 1987. On the derivation of thermomechanical balance equations for continuous systems with a nonmaterial interface. Int. J. Eng. Sci. 25, 1459–1468.

Dell'Isola, F., Sciarra, G., Batra, R.C., 2003. Static deformations of a linear elastic porous body filled with an inviscid fluid. J. Elast. 72, 99–120.

Dell'Isola, F., Seppecher, P., Madeo, A., 2012. How contact interactions may depend on the shape of Cauchy cuts in *N*-th gradient continua: approach ''à la D″Alembert". Z. Angew. Math. Phys. (ZAMP), 1–23.

Eremeyev, V.A., Pietraszkiewicz, W., 2009. Phase transitions in thermoelastic and thermoviscoelastic shells. Arch. Mech. 61, 41–67.

Eremeyev, V.A., Pietraszkiewicz, W., 2011. Thermomechanics of shells undergoing phase transition. J. Mech. Phys. Solids 59, 1395–1412.

Feng, W., Yang, W.H., 1973. On the contact problem of an inflated spherical nonlinear membrane. J. Appl. Mech. 41, 209–214.

Hirdaris, S.E., Temarel, P., 2009. Hydroelasticity of ships: recent advances and future trends. Proc. Inst. Mech. Eng. Part M J. Eng. Marit. Environ. 223 (3), 305–330.

Lemaitre, J., Chaboche, J.L., 1998. Mechanics of Solid Materials. Cambridge University Press.

Ligarò, S.S., Barsotti, R., 2008. Equilibrium shapes of inflated inextensible membranes. Int. J. Solids Struct. 45, 5584–5598.

Luongo, A., Rega, G., Vestroni, F., 1984. Planar non-linear free vibrations of an elastic cable. Int. J. Linear Mech. 19, 39–52.

Mc Crum, N.G., Buckley, C.P., Bucknall, C.B., 1997. Principles of Polymer Engineering. Oxford University Press.

Nadler, B., 2010. On the contact of spherical membrane enclosing a fluid with rigid parallel planes. Int. J. Non Linear Mech. 45, 294–300.

Qi, H.J., Boyce, M.C., 2005. Stress-strain behavior of thermoplastic polyurethan. Mech. Mat. 37, 817–839.

Quiligotti, S., Maugin, G., dell'Isola, F., 2003. An Eshelbian approach to the nonlinear mechanics of constrained solid-fluid mixtures. Acta Mech. 160, 45–60.

Rinaldi, A., Correa-Duarte, M.A., Salgueirino-Maceira, V., Licoccia, S., Traversa, E., Dávila-Ibáñez, A.B., Peralta, P., Sieradzki, K., 2010a. In-situ micro-compression tests of single core-shell nanoparticles. Acta Mater. 58 (19), 6474–6486.
Rinaldi, A., Licoccia, S., Traversa, E., Sieradzki, K., Peralta, P., Dávila-Ibáñez, A.B., Correa-Duarte, M.A., Salgueirino, V., 2010b. Radial inner morphology effects on the mechanical properties of amorphous composite cobalt boride nanoparticles. J. Phys. Chem. 114 (32), 13451–13458.
Ross, E.C., Simmons, C.A., 2007. Introductory Biomechanics from Cells to Organisms. Cambridge University Press.
Sohail, T., Nadler, B., 2011. On the contact of an inflated spherical membrane-fluid structure with a rigid conical indenter. Acta Mech. 218, 225–235.
Yokota, J.W., Bekele, S.A., Steigmann, D.J., 2001. Simulating the nonlinear dynamics of an elastic cable. AIAA J. 39, 3.